Facile encapsulation of glabridin in Zeolitic Imidazolate Framework-8 (ZIF- 8): Characterization, antibacterial activity and in-vitro drug release

Safdar Ali Amur

safdaraliamur@gmail.com

Beijing University of Chemical Technology

Najaf Ali Soomro

University of Sindh

Quratulain Khuhro

University of Sindh

Mingxia Wang

Beijing University of Chemical Technology

Muhammad Tariq

Beijing University of Chemical Technology

Junaid Munwar

Beijing University of Chemical Technology

Naveed Karim

Beijing University of Chemical Technology

Hao Liang

Beijing University of Chemical Technology

Research Article

Keywords: Glabridin, ZIF-8, Encapsulation, Antibacterial, drug release

Posted Date: April 5th, 2024

DOI: https://doi.org/10.21203/rs.3.rs-4183387/v1

Additional Declarations: No competing interests reported.

Abstract

In this research, a natural bioactive glabridin (Glab) flavonoid compound was encapsulated in zeolitic imidazolate framework-8 (ZIF-8) via one-pot technique at room temperature. Herein, ~98.7% of drug was encapsulated into ZIF-8 coreshell, which depicted 28.44% drug encapsulation productivity of ZIF-8. Fourier transform infrared (FTIR), UV—Vis spectroscopy and X-ray crystallography (XRD) confirmed the drug encapsulation. Next, the newly constructed nanomaterials were greatly studied with, dynamic light scattering (DLS), scanning electron microscope (SEM), energy-dispersive X-ray (EDX) analysis, transmission electron microscope (TEM) and thermo gravimetric analysis (TGA) technologies. SEM and TEM showed hexagonal morphology of Glab@ZIF-8 and an increased particle size to that of ZIF-8 i.e., 138.62±5.4 nm and 91.69±6.2 nm, respectively. TGA depicted 32.14% Glab@ZIF-8 material's decomposition at 644 °C. The antibacterial efficacy of Glab@ZIF-8 was found superior against *S. aureus* than *E. coli* and *Bacillus subtilis*, resulting 26±0.01 mm, 23±0.02 mm and 11±0.01 mm inhibition zones and MIC values 31.2 µg, 62.5 µg and 125 µg, separately. Though, the Glab@ZIF-8 kept in an acidic medium (pH 5) for 72 h showed highest drug release 89.76% as compared to the pH 5.5 (81.23%) and pH 7.4 (24.78%). In conclusion, ZIF-8 remained a potential drug delivery system and Glab@ZIF-8 nanocomposite can be accredited for broader biomedical applications to cure infection diseases and malignant cells.

1. Introduction

Human life has been affected by infectious diseases since prehistoric times. Alexander Fleming, who discovered penicillin in 1923, promised the eradication of infectious diseases. However, since then, the overuse and uncontrolled use of antibiotics have led to an increase in the incidence of bacteria resistant to these drugs [1]. Therefore, the development of antibiotic resistance in bacteria represents a serious health threat. The world may soon experience a "postantibiotic" scenario, according to a universal antimicrobial resistance map released by the World Health Organization (WHO) [2]. Furthermore, a global health catastrophe has resulted from the extraordinary increase in the prevalence of antibiotic-resistant bacteria; an estimate indicates that by 2050, up to 10 million people could die annually. In addition to the virulence of pathogens, which can cause illness and death, antibiotic resistance is thought to be one of the most important possible variables in patients with severe infections. It is believed that both gram-positive and gram-negative bacteria are resistant to antibiotics [3]. Wide-spectrum medications may help prolong the resistance cycle insofar as the overuse of antibiotics has resulted in adaptational resistance [4, 5]. However, gram-negative microbes require substantial attention because they have developed resistance to multiple drugs. Because this issue keeps worsening, it is necessary to look for alternate microbiological medication. In the present era, for the improvement of public health, especially in the case of infectious diseases, new antimicrobial compounds originating from terrestrial or aquatic sources with a broader spectrum of activities must be applied and improved via the help of nanotechnology to minimize the drug resistance of bacteria [6].

A meaningful flavonoid called glabridin (Glab) is chiefly isolated from the roots of the traditional herb *Glycyrrhiza glabra* (Licorice) [7]. Its systematic name is (4-[(3*R*)-8,8-dimethyl-3,4-dihydro-2*H*-pyrano[2,3-*f*]chromen-3-yl]benzene-1,3-diol, $C_{20}H_{20}O_4$). The literature addressing its chemical and biological characteristics has multiplied rapidly since its initial isolation and characterization in 1976. It has significantly impacted many industries, such as food, cosmetics, dietary supplements, and medications. According to previous reports, glabridin's pharmacological actions reduce metabolic irregularities, which ultimately reduces the risk of obesity, cardiovascular disease and diabetes [8, 9]; protect the nervous system; help to prevent abnormalities; act as an estrogen substitute [9]; prevent *Staphylococcus*, *Candida*, *Helicobacter pylori* and other bacterial infections [10, 11]; and act as a safe anticancer agent [12], anti-inflammatory agent [13], antiosteoporosis agent [14], etc. However, glabridin, despite its clinical significance and future broader pharmacological bioapplications, is not free from certain restrictions, such as structural stability, which can be greatly influenced by temperature, radiation, pH, humidity, and the nature of the solvent [15], leading to limited applications. Furthermore, glabridin has been shown in earlier investigations to degrade at room temperature in the presence of natural light [15, 16], which shortens its shelf life. However, its storage requires special efforts, such as in a dark, dry and oxygen-free environment [15]. Additionally, its hydrophobicity (not soluble in water) decreased its absorption in vivo, resulting in low bioavailability and thus limiting its clinical application [15]. On the other hand, it is incompatible with physiological pH; for example, it remains unstable under basic conditions (pH > 7), the structures of its degradation products are yet unknown [15], and it remains stable only at neutral pH [15]; moreover, its further pharmacological value is lacking [17]. However, such limitations to glabridin could be handled through encapsulation technology [17–20], as it is widely considered a leading alternative for protecting, stabilizing and delivering bioactive drugs with the aid of pH-responsive media [18]. Furthermore, the shelf life of bioactive natural drugs can be improved at normal temperatures, and their decomposition by environmental factors can be limited if they can be loaded into advanced nanomaterials, i.e., metal-organic frameworks [21], by adopting novel nanotechnology strategies.

Nanotechnology involves the synthesis of nanomaterials (seized between 1 and 1000 nm) for various applications, such as biomedicines, catalysis, food technology, electrochemistry and pharmaceutics. [22]. Due to their chemical, optical and biological efficacy, nanomaterials have gained unique attention in biomedical studies [23]. Among the numerous reported nanomaterials, metal-organic frameworks (MOFs) [24], owing to their versatile structures, well-defined pores, tunable components and high surface areas [25], are widely considered promising drug transporters, catalysts, sensors, and separation/adsorbing agents. On the other hand, the zeolitic imidazolate framework-8 (ZIF-8) MOF, which belongs to the well-known ZIF family, is highly famous among researchers who work on drug delivery systems. Seel and coworkers synthesized ZIF-8 (a Zn and 2-methylimidazolate) for the first time in 1980 [26, 27]. ZIF-8 has a high surface area, large (11.6 Å) pore size [27], elevated chemical and thermal stabilities, and robust porosity [25]. Additionally, the structural components of ZIF-8, i.e., Zn^{2+} and an organic linker (2-methyl imidazolate), are bioconsumable materials. In biological systems, zinc is the subsequent very typical transition element, and the imidazole group is a crucial component of the amino acid histidine [28]. ZIF-8 is documented to be an effective drug delivery vehicle [18–20, 27], as it has a

large encapsulating capacity, and its tiny pore size (3.4 Å) prevents early drug release [29]. Furthermore, ZIF-8 has strong dispersibility, while it undergoes deprotonation between pH 5 and 6; hence, it could be used for the controlled release of drugs at the targeted site[29–32]. Considering recent studies, ZIF-8 was the most suitable drug delivery system for diseased cells where the microenvironment was acidic (pH 5.0–6.8) compared to healthy tissues and blood circulation [33]. ZIF-8, in view of the above qualities, has been widely studied as a potentially useful material for the encapsulation and pH-responsive shipment of various medicines [18], nucleic acids, fluorescein [34], photothermal agents [35, 36] and active proteins [37] owing to its certain shortcomings. Furthermore, several previous recent studies have reported the encapsulation of curcumin [20], physcion [18] and gentiopicroside [19] into ZIF-8 to improve drug stability and pharmacokinetics and to observe enhanced antibacterial activity.

In this study, a greener approach was adopted to encapsulate the natural flavonoid glabridin into ZIF-8. Therefore, based on the dry weight of the materials used, a 38.5% yield of the Glab@ZIF-8 nanomaterial (138.62 ± 5.4 nm) was obtained. Moreover, the drug loading capacity of ZIF-8 was 28.44%, and the drug encapsulation capacity was ~ 98.7%. High drug release (89.76%) was achieved in an acidic medium compared to that in a physiological medium in an in vitro experiment, revealing the prominent ability of ZIF-8 to deliver certain drugs into diseased cells. These findings could also be referenced while designing in vivo studies in the future. Moreover, in the antibacterial study, Glab@ZIF-8 had a greater growth inhibition zone (26 ± 0.01 nm) for *S. aureus* bacteria than for *E. coli* (23 ± 0.02 mm), for which the MIC was 31.2 µg or 62.5 µg. Consequently, newly prepared Glab@ZIF-8 nanocomposite can be broadly accepted for biomedical applications to combat drug-resistent microbes and malignant cells.

2. Materials and methods

2.1. Chemicals

Zinc nitrate hexahydrate (**$Zn(NO_3)_2 \cdot 6H_2O$**) 98% pure and 2-methylimidazole (purity 99%) were purchased from Aladdin Ltd. (Shanghai, China). Glabridin (98% pure) was procured from Jiamu Biotechnology (Hunan, China). Hydrochloric acid (HCl), ethanol, phosphate-buffered saline (PBS), tween-80 and other chemical reagents of analytical quality were obtained from Beijing Chemical Works, Beijing, China.

2.2. Synthesis of Glab@ZIF-8 and ZIF-8 nanomaterial

The Glab@ZIF-8 was synthesized through the one-pot method [18, 19]. In detail, 1 g of $Zn(NO_3)_2 \cdot 6H_2O$ and 2.5 g of 2-methylimidazole were dissolved in 20 mL of Milli-Q water, separately, and were stirred at room temperature for 30 minutes to obtain a clear solutions. Likewise, 10 mg of glabridin was skillfully dissolved in 10 mL of ethanol. Thereafter, the 2-methylimidazole solution was stirred using a magnetic stirrer and preheated at 27°C and 800 rpm; subsequently, zinc nitrate and glabridin solutions were gradually added. The reaction mixture hue was altered from a transparent solution to a milky turbid solution in approximately 10–15 seconds, indicating the synthesis of the Glab@ZIF-8 framework nanomaterial. In parallel, a ZIF-8 framework nanomaterial, which is a drug-encapsulating nanocarrier,

was also synthesized for comparative analysis through the same protocol except for the addition of a glabridin solution. The resultant nanomaterial was further allowed to react for 30 minutes under predefined conditions. Consequently, both nanomaterial solutions were centrifuged through a refrigerated (4°C) centrifuge (H1750R, Xiangyi/Cennia) at 10000 rpm for 12 minutes. The precipitates of the nanomaterials were washed with water and ethanol three times to remove unreacted chemicals. Finally, powdered material was obtained through lyophilization (Alpha 1–2 LDplus, Christ/Sigma) under vacuum conditions at –55°C for 12 hours.

The drug loading encapsulation (DLE) and drug loading capacity (DLC) [18–20] of the ZIF-8 framework were estimated by dissolving a suitable amount of Glab@ZIF-8 in 1 M HCL (200 µL) and subsequently diluting the mixture to 2 mL with ethanol. The supernatant was studied spectrophotometrically at 282 nm [38] to determine the absorbance of glabridin. The concentration of free drug was calculated using the standard calibration curve of glabridin plotted against different concentrations, i.e., 12.5 µg to 1000 µg (**Figure S1**), which was calculated via the regression analysis equation y = 0.003x + 0.3176 (R^2 = 0.9955). The following formulas were applied:

$$DLE\,(\%) = \frac{(amountofloadeddrug)}{(amountoffeededdrug)} \times 100$$

$$DLC\,(\%) = \frac{(amountofloadeddrug)}{(amountofdrugloadedNPs)} \times 100$$

2.3. Characterization of the synthesized materials

UV–Vis spectra of Glab@ZIF-8 and ZIF-8 aqueous and glabridin-ethanol solutions were obtained with a UV-2450 spectrophotometer (Shimadzu, Kyoto, Japan). The zeta potential and dynamic light scattering (DLS) density of Glab@ZIF-8 and ZIF-8 were measured through a Malvern Zetasizer (Nano ZS). FTIR spectra of all the materials were recorded with a Nicolet 6700 FT-IR spectrometer (Thermo Fisher Scientific, Waltham, MA, USA) with a DLaTGS detector in the range of 4000 ~ 500 cm^{-1} through the KBr tablet press method. Powder X-ray diffraction (XRD) analysis of the materials was performed using a Bruker D8 Advance powder X-ray diffractometer (Germany), and the copper target X-ray tube was run with Cu Kα radiation at 40 kV and 40 mA. Scanning of the samples ended at a scan frequency of 10°/min in the 2θ range (from 5° — 60° with a 0.02° step size). The morphology of the synthesized materials was assessed by scanning electron microscopy (SEM) (HITACHI S-4700, Japan) at 0.5 ~ 30 kV and transmission electron microscopy (TEM) (HITACHI, HT7700, Japan) at 120 kV. For SEM analysis, the sample material was suspended in deionized water; thus, one drop of diluted sample was added to the carbon-coated double-sided adhesive tape, which was prefixed onto the brass stub sample holder. Subsequently, the sample was allowed to dry (~ 8 h) and then sprayed with a reedy gold layer for electrical conductivity. The EDX analysis was also performed through the SEM via EDAX software analyzer. For the TEM analysis, one drop of material dispersed in deionized water was applied to a copper mesh grid and subsequently dried overnight, after which the samples were analysed.

2.4. Thermal stability of synthesized materials

Thermogravimetric analysis (TGA) of synthesized Glab@ZIF-8, ZIF-8 and glabridin was performed with a thermal analysis system (Hitachi STA7300). The samples were placed in platinum pans. Thus, the samples were heated between 34 and 800°C at 10°C/min with a nonstop supply of nitrogen gas (50.0 mL/min).

2.5. Antibacterial activity of synthesized materials

Bacterial strains, such as *Staphylococcus* (S) *aureus*, *Bacillus subtilis* (JCL16) and *Escherichia coli (E. coli*: BW25113/F), were obtained from the College of Life Science and Technology, Beijing University of Chemical Technology, Beijing, China. The antibacterial activity of the materials was assessed using Luria–Bertani (LB) agar growth media [39] via the well diffusion method [18, 19]. In detail, the media were prepared by dissolving 5 g of peptone, NaCl and yeast extract (2.5 g) in 0.5 L of ultrapure H_2O. An equal volume of media solution was poured into 5 conical flasks, and 2 g of agar was added to 4 flasks while leaving one flask as LB broth media, which was used to grow the bacterial culture. The media was autoclaved at 115°C for 20 minutes. Fresh bacterial cultures were prepared by adding 10 µL of strain stock to 4 mL of LB broth media and incubating at 37°C with continuous shaking at 200 rpm for 8 hours. For each corresponding bacteria, ~ 30 mL of LB agar growth media was drained into 60 mm sterilized petri dishes under ambient conditions using a biosafety cabinet. The prepared plates were left to solidify for 40–45 minutes. One hundred microliters of fresh bacterial culture was applied to each corresponding plate, which was spread finely with a glass spreader and allowed to saturate/adsorb for 10 minutes. Thereafter, the wells in the plates were made through a sterilized 6 mm metal cork borer. Stock solutions of materials such as Glab@ZIF-8, glabridin, ZIF-8 and the known antibiotic ampicillin were prepared by diluting 500 µg/mL in 50% dimethyl sulfoxide (DMSO) solution. For antibacterial testing, 50 µL of Glab@ZIF-8 and ampicillin, whereas, 100 µL of glabridin and ZIF-8 stock solutions, were added to prelabelled wells on agar media plates and subsequently incubated at 37°C for up to 24 hours. The developed zones that restrict growth around each well were gauged in mm, the length of the hole was measured (i.e., 6 mm), and the final results are presented as the means ± SDs of triplicate samples. The minimum inhibitory concentration (MIC) of Glab@ZIF-8 nanoparticles was done as reported somewhere [40]. For this a 10 10 µL of fresh bacteria culture were added to 4 mL LB media in test tubes, thus, a different concentartions (µg/mL) of Glab@ZIF-8 were loaded. MIC assays were incubated at 37°C for 24 hours with constant shaking at 200 rmp. Next, the MIC values were reported by observing visual turbidity in each test tube.

2.6. In vitro pH-dependent drug release profile

Drug release i.e., glabridin from Glab@ZIF-8 was studied at pH 5, pH 5.5 and pH 7.4 for 1 hour to 72 hours. The analysis was performed according to previous methods [18, 19] with slight modifications. For each pH, 5 mg of Glab@ZIF-8 material was poured into 50 mL centrifuge tubes, after which 30 mL (20 mM) of phosphate buffer saline (PBS) containing 10% ethanol and the surfactant tween-80 (0.5% v/v) were added, after which the mixture was mixed well. The solutions were shaken (200 rpm) and preset at

37°C. Subsequently, after each defined interval, a 1 mL aliquot of the mixture sample was pipetted for centrifugation; hence, the same volume of pure PBS was added to the corresponding mixture. The concentration of the released drug was studied spectrophotometrically at 282 nm, and the results are expressed as the cumulative release percentage at each time interval.

2.7. Statistical analysis

Origin Pro software (version 2022) was used to assemble the data once the triplicate experimental investigation was completed. The numerical data are expressed as the mean ± standard deviation of replication or as a percentage (%).

3. Results and discussion

3.1. Synthesis of nanomaterials

In this study, Glab@ZIF-8 and ZIF-8 materials were synthesized through a greener approach, the “one-pot technique”, as illustrated in Fig. 1. In comparison to the other typical methods, the one-pot synthesis method is more convenient for handling raw materials at a smaller scale and is feasible for obtaining the resultant material at low cost, energy and time [41]. In addition, the one-pot strategy significantly reduces the number of reactions [41]. In the case of environmentally friendly ZIF-8, this method requires only zinc metal ions and 2-methylimidazole (as an organic linker) solutions in deionized water. During the mixing of these two solutions at room temperature (27°C) and at the specified times, porous structures with hollow cavities are generated [41]. For Glab@ZIF-8, the drug solution was made into ethanol, which was subsequently added to the ZIF-8 solution system. This approach allows guest molecules to be trapped in cavities of ZIF-8 core shells, which may cause stretching and an increase in the size of the core shell structure of the composite (Glab@ZIF-8) compared to that of pure ZIF-8 [41]. In this study, ZIF-8 or Glab@ZIF-8 nanocomposite synthesis was observed within a few seconds (~ 15), as the transparent solutions were immediately turned into milky solutions [18, 19]. The yield of Glab@ZIF-8 based on dry weight was 38.5%. However, in the single-step synthesis of Glab@ZIF-8, a 28.44% loading efficiency was found for glabridin, and the drug loading encapsulation efficiency was ~ 98.7%. The high drug loading of glabridin into ZIF-8 frameworks could be attributed to the large pore size [27], robust porosity [25] of ZIF-8 and robust contact between the guest (glabridin drug) and host (ZIF-8) [42].

3.2. Characterization of ZIF-8 and Glab@ZIF-8 nanomaterials

The encapsulation of glabridin within the ZIF-8 i.e., Glab@ZIF-8 nanomaterial was confirmed through UV–Vis spectroscopy and FTIR spectroscopy. Figure 2 (**a**) shows that glabridin exhibited a maximum UV–Vis absorption peak at 283 nm, which is consistent with the findings of previous studies [38, 43]. ZIF-8 had a maximum UV–Vis absorption peak at a wavelength of 211 nm [44, 45]. Compared with that of ZIF-8, the UV–Vis absorption peak of Glab@ZIF-8 was redshifted at 222 nm, and the characteristic

absorption peak of glabridin was masked. This confirmed the encapsulation of the drug (glabridin) into the ZIF-8 framework [18–20, 46]. The entrapment and interaction between the drug and ZIF-8 are subjected to various forces, such as electrostatic interactions, π-π interactions or strong hydrogen bonds between guest (glabridin) and host (ZIF-8) molecules [18, 19, 42]. FTIR analysis of pure glabridin (Fig. 2b) revealed O − H stretching in the IR spectrum, with a maximum absorption peak at 3390 cm^{-1} [38]. The peak at 2974 − 2922 cm^{-1} represents the CH_3 group [38]. The peak at 1744 − 1463 cm^{-1} might be attributed to the C–C stretching vibration of the aromatic ring [38]. The peak at 1370 − 1329 cm^{-1} is due to deformation vibration, and the peak at 1215 − 1152 cm^{-1} is attributed to C-O-C stretching. It has also been reported that the peak at 1080 − 945 cm^{-1} corresponds to C-O stretching vibrations and that the peak at 851 − 706 cm^{-1} may correspond to O-H bending [38]. The ZIF-8 IR spectrum, as presented in Fig. 2 **(b)**, depicted N-H stretching and C-H aromatic stretching at absorption peaks from 3431 − 3099 cm^{-1} [47] and C—H stretching [18] within 2916–2922 cm^{-1}. However, a peak at 2844 cm^{-1} is assigned to the vibrational stretch of the methyl group contained in 2-methylimidazole [19]. Moreover, representative peaks at 1744 cm^{-1}, 1679 − 1656 cm^{-1} and 1562 − 1428 cm^{-1} attributed to ZIF-8 were attributed to the C-C and C–N stretching of imidazole and entire ring stretching, respectively [18, 19, 47]. The peak at 1386 − 681 cm^{-1} is also attributed to the 2-MIM ring [47, 48]. The Glab@ZIF-8 composite material exhibited similar peaks to those of ZIF-8 (Fig. 2b). However, compared with those of the pure ZIF-8 peak, the broad peak at 3503 − 3410 cm − 1 is blueshifted (3746 cm − 1, 3431 cm − 1), and a redshift can be observed compared to the broad absorption peak at 3390 cm^{-1}. Consequently, this pattern showed the encapsulation of glabridin in ZIF-8 frameworks [18, 38, 49]. Furthermore, other distinctive peaks of pure glabridin were obscured by the Glab@ZIF-8 material [38].

The DLS study showed that the mean hydrodynamic diameter sizes of ZIF-8 and Glab@ZIF-8 were 103.19 nm and 146.03 nm, respectively (Fig. 2c, d). The diminished dimensions of nanoparticles (NPs) confer significant advantages in biomedical applications, particularly due to their enhanced suitability and efficacy [50]. On the other hand, the increase in the size of the Glab@ZIF-8 material to that of ZIF-8 [29] also confirmed drug encapsulation. Furthermore, ZIF-8 exhibited a + 35.17 mV zeta potential (ζ), and Glab@ZIF-8 also exhibited a + 41.9 mV zeta potential (Fig. 2e). Therefore, the absence of any electrical charge and a slightly increased zeta potential also indicate the encapsulation of glabridin in ZIF-8 [46]. High zeta potential values indicate that these nanoparticles are well dispersed and stable in water and PBS (pH 7.4) [46]. Additionally, it has been reported that ζ-potentials of NPs within ± 30 to ± 40 mV indicate moderate electrostatic stability, although ζ-potentials above ± 40 mV reveal strong electrostatic stability [51]. Subsequently, in the present study, Glab@ZIF-8 NPs were prepared with increased stability and could also be stored in suspension at room temperature [51]. Moreover, TEM analysis based nanoparticle size of ZIF-8 was 91.69 ± 6.2 nm (Fig. 2f). However, Glab@ZIF-8 had an average size of 138.62 ± 5.4 nm (Fig. 2f). An increase in size results from the loading of drug molecules into MOF cavities.

The morphology of the prepared materials was studied through TEM and SEM. The nanosized ZIF-8 structure as developed by TEM and SEM is homogeneous, uniform and hexagonal as shown in Fig. 3 **(a,**

c). Similarly, the morphology of Glab@ZIF-8 as depicted in Fig. 3 **(b, d)** is analogous to that of ZIF-8. Furthermore, the TEM image of Gla@ZIF-8 revealed that the material has sharp edges, which are highly favorable for certain antibacterial applications [52–54]. The elemental composition of ZIF-8 and Glab@ZIF-8 nanomaterials was analyzed EDX via SEM technique using EDAX software. It can be seen in Fig. 4 **(a)** that ZIF-8 has an elemental composition of 21.95 % zinc(Zn), 34.82 % carbn (C), 17.37 % nitrgen (N) and 19.01 % oxygn (O). In contrast, Glab@ZIF-8 as shown in Fig. 4 **(b)** has 19.09 % Zn, 9.61 % C, 1.27 % N an 14.24 % O inrespect of elemental composition. It is supposed that after loading of glabridin into ZIF-8 frameworks (Glab@ZIF-8), the weight % of Zn was reduced, while, the weight % of C was increased to that of ZIF-8. Yet the weight % of O and N was also oscillated. This phenonmenon also demonstrated the loading of drug into ZIF-8 nanoparticles [55, 56].

The loading of glabridin into ZIF-8 was also explored by comparing the powdered XRD pattern of the pure materials with that of the synthesized material (Fig. 5). XRD is widely applied as an absolute technique for observing the crystal structure of certain materials [57]. The XRD pattern of ZIF-8 showed 2θ clear sharp characteristic peaks at 7, 9, 10, 11, 11.6, 12.4, 13, 16, 17, 18, and 18.6 diffraction angles, which are similar to reported works [18, 58] and are inconsistent with the planes indices 110, 200, 112, 022, 013 and 222, respectively [18, 19]. Other 2θ peaks in ZIF-8 were observed at 20, 22, 22.7, 23.3, 24.6, 25.9, 27, 27.7, 28, 29.3, 30, 32, 33, 34, 35, 36.6, 38, and 40 cm^{-1} diffraction angles. Thus, the material ZIF-8 is in its pure phase and crystalline [18]. Here, the XRD pattern of pure glabridin was consistent with that of previously reported studies [38]. The characteristic 2θ peak values were observed at 8.5 10, 12, and 18 [38], where diffraction angles appeared. However, other 2θ peaks at 43.28 and 44.4° were also noted. Moreover, similar 2θ peaks were observed for Glab@ZIF-8, although the 2θ peaks at 8.5 10, 12, and 18 cm were masked by the Glab@ZIF-8 composite. This could result from the loading of drugs into the cavities of ZIF-8 frameworks [20, 42, 59]. Likewise, the XRD pattern of Glab@ZIF-8 was consistent with that of pure ZIF-8; henceforth, the composite material had a crystalline structure and was found to be a pure phase [18, 60].

3.3. Thermal stability of ZIF-8 and Glab@ZIF-8 nanomaterials

The Fig. 6 illustrates the thermal stability of Glab@ZIF-8, ZIF-8, and glabridin. Glab@ZIF-8 exhibited a 1.43% initial weight loss at 145°C, which was due to the removal of any solvent [18, 19, 61]. Afterwards, an 8.86% (at 214°C) weight loss was attributed to the primary decomposition of the MOF ring structure [18, 19, 61]. Moreover, Glab@ZIF-8 degraded 12.03%, 18.65% and 32.14% at 251°C, 450°C and 644°C, respectively. Henceforth, 67.86% of the Glab@ZIF-8 particles were estimated to remain stable even at the highest temperature. It is assumed that at high temperatures, 2-methylimidazolate is completely burned; therefore, the decomposition of ZIF-8 occurs. In contrast, glabridin gradually degraded at 50°C, 92°C and 293°C, as indicated by weight loss values of 1.87%, 4.96% and 5.85%, respectively. Complete degradation of glabridin was considered up to ≥ 365°C, as the weight loss was 79.12%. In contrast, ZIF-8 remained stable between 76°C and 260°C, so minimal weight losses of 1.84% and 10.71%, respectively, were observed. However, gradual degradation of ZIF-8 occurred at 286°C (23.53%), 466°C (28.36%) and

598°C (30.57%). In conclusion, the encapsulation of biomaterials in ZIF-8 frameworks could be considered to modify and improve their thermal stability, and their shelf life could also be extended for a longer time at room temperature.

3.4. Study of antibacterial activity

Humans are easily infected by many pathogenic organisms in communal settings and via the consumption of contaminated food. Among human pathogens, *Bacillus cereus* and *Escherichia coli* cause gastroenteritis, *Staphylococcus aureus* is responsible for skin and soft tissue infections, and *Pseudomonas aeruginosa* causes infections in burn patients. It has been documented that these bacteria may produce resistant biofilms; colonize wounds, implants, and medical equipment; and frequently cause morbidity and death [62]. The overprescription and excessive use of antibiotics have led to multidrug resistance among bacteria. Henceforth, the ongoing development of substitute antibacterial agents for traditional antibiotics is a major task. Natural antibacterial agents obtained from animals, plants, algae, fungi and bacteria are of great interest as substitutes for typical antibiotics [63]. Additionally, natural bioactive compounds are “generally acknowledged as secure” and have a “greener” impact on consumers. Plant-originated antimicrobial agents have long-term value in the healthcare market because they satisfy customers' growing need for environmentally friendly products, hence enhancing the importance of researching new, promising biopharmaceutical products [63]. For example, glabridin is a crystalline compound enriched in numerous biological applications, including antibacterial potential [64]. The suboptimal pharmacokinetic characteristics and inadequate stability of glabridin restrict its potential therapeutic applications. Consequently, in response to advancements in nanotechnology, medicinal and synthetic chemists have embraced the strategy of developing drug-based metal-organic frameworks (MOFs) to address the limitations associated with naturally occurring bioactive compounds. Previous research has documented the effectiveness of natural drug-based nanomaterials in combating drug-resistant bacteria [18, 19].

The antibacterial activity of the tested materials is given in Fig. 7 **(a, b, c)**. The findings of this study illustrate that 25 µg/50 µL of Glab@ZIF-8 had additional comprehensible growth inhibition effects on *S. aureus*, followed by *E. coli* and *Bacillus subtilis*, with growth inhibition zones of 26 ± 0.01 mm, 23 ± 0.02 mm and 11 ± 0.01 mm, respectively. However, compared with Glab@ZIF-8, glabridin and ZIF-8 (50 µg/100 µL) exhibited almost half the restriction on the growth of *S. aureus*, *E. coli* and *Bacillus* subtilis (**table S1**). Subsequently, growth inhibition zones of 15 ± 0.03 mm and 17 ± 0.01 mm, 12 ± 0.01 mm and 13 ± 0.03 mm and 7 ± 0.01 mm and 7.9 ± 0.01 mm were noted for glabridin and ZIF-8, respectively. Nevertheless, 25 µg/50 µL of ampicillin suspension had 27 ± 0.03 mm, 23 ± 0.03 mm and 20 ± 0.01 mm growth inhibition zones for *S. aureus, E. coli* (BW25113/F), and *Bacillus subtilis* (JCL16), respectively. In conclusion, the improved antibacterial efficacy of Glab@ZIF-8 compared to that of the natural compounds glabridin and pure ZIF-8 is attributed to the synergistic mechanism of action. Furthermore, encapsulation of similar drugs in MOFs could be used to formulate new alternative antibacterial materials, and this strategy would be highly helpful for reducing the prevalence of MDR bacteria. Nevertheless, an important benefit would be that microbes should not be as likely to become resistant to

these newly synthesized nanomaterials, as they might harbor more than one bactericidal target [63]. The MIC values for *S. aureus* and *E. coli* were 31.2 µg (Fig. 7d) and 62.5 µg (Fig. 7e), respectively. However, 125 µg was the MIC against *Bacillus subtilis* (Fig. 7f). The MIC assay results are in agreement with the antibacterial growth inhibition assay results. The results of this study revealed that Glab@ZIF-8, ZIF-8 and glabridin were more effective against gram-positive *S. aureus* bacteria than against gram-negative *E. coli* bacteria. As far as *Bacillus subtilis*, which is reported to be a highly drug-resistant bacterium [65], high doses of the tested materials were effective compared to those of *S. aureus and E. coli.*

Somewhere, it was stated that glabridin exhibited antimicrobial activity against *Helicobacter pylori* and methicillin-resistant *Staphylococcus aureus* [64]. Furthermore, 29.16 g (1 mL) showed antitubercular activity against *Mycobacterium* [64]. Glabridin was also more effective against gram-positive microbes than against gram-negative microbes [64]. These findings support and authenticate the results of the present study. Moreover, glabridin contains two free phenolic hydroxyl groups at the 1,3-position, which may strengthen its antibacterial potential [64]. On the other hand, ZIF-8 contains Zn^{2+} and 2-methylimidazole, so Zn^{2+} may penetrate bacterial cell walls easily [66, 67] or 2. Methylimidazole can attach to the cell wall, causing the membrane to tear, distort, and release cytoplasmic substances [18, 19]. However, in the case of MOF interactions with the cell matrix, Zn^{2+}, drugs and 2-methylimidazole released from MOFs could intermingle with bacterial enzymes and may inhibit respiratory reactions [18, 19]. Additionally, 2-methylimidazole can attach to protein-SH groups, which can cause bacterial cell death [18, 19]. Currently, Zn^{2+} composites containing imidazole linker derivatives have gained considerable recognition for their antibacterial properties [18, 19]. On the other hand, metallic nanomaterials may cause pits or holes in the bacterial cell wall, which in turn permits the entry of NPs into the cell matrix or the rupture of the cell membrane, allowing integral material to leak and cause cell death. In recent years, nanoantimicrobials have been shown to have different mechanisms of action for both types of bacteria. Researchers have documented low drug resistance in *S. aureus* following infection with *E. coli* due to the cell wall composition [68]. *S. aureus* has only a single layer of cytoplasmic membrane attached to peptidoglycan sheets, which exhibit chains of linear polysaccharides divided by brief peptides, where lipoteichoic acids adhere. The difference in cell walls could also be attributed to differences in antibacterial activity [69]. As a result, cell membranes become anionic and amphiphilic. Henceforth, metal ions and bioactive compounds can easily bind to the cell membrane or enter the cytoplasm and can produce reactive oxygen species or bind to SH- groups of genetic material, ultimately resulting in cell death [19, 69]. Considering these findings, *S. aureus* is considerably less drug resistant than is *E. coli*, whereas the *E. coli* peptidoglycan layer between the cell wall and cytoplasm contains lipopolysaccharides, which hinder the entry of certain chemicals [19, 68], and the additional periplasmic space between layers contains few enzymes that may also breakdown extracellular substances [68, 70]. *E. coli* has a high level of drug resistance because different outflow pumps in cell membranes effectively lower the concentration of such medicines within the cell [68]. In addition, it is accepted that smaller metallic nanoparticles provide better interactions between NPs and bacterial cell walls, thus allowing them to rupture membranes and develop the highest antibacterial efficacy [71]. In this study, the nanosized prepared material (as shown in Fig. 5) exhibited distinct sharp edges attributed

to the presence of zinc metal. Consequently, it is postulated that this particular morphology holds the greatest potential for exerting antibacterial activity. Mechanically, as bacteria interact with materials, sharp edges will destroy cell walls [52–54]. In conclusion, Glab@ZIF-8 demonstrated the highest level of antibacterial activity against microorganisms, suggesting that this medication may be useful for treating illnesses related to microbial infections and may be helpful in biomedical applications based on nanomaterials.

3.5. In vitro pH-dependent drug release profile

This study investigated the release profile of the drug glabridin from Glab@ZIF-8 in different pH environments and in tween-80 solutions (Fig. 8). The results showed that the highest drug release (89.76%) occurred at pH 5 after 72 hours, followed by 81.23% at pH 5.5 and 24.78% at pH 7.4. This high drug release under acidic conditions is attributed to the protonation of the imidazolate ring of ZIF-8 [18, 19, 32], which breaks the coordination of the metal framework and allows the drug to be released [18]. In contrast, under basic conditions, ZIF-8 remains stable, resulting in slower drug release [18, 19, 32]. The drug release process is also time dependent, further confirming the stability of the MOF. The study also revealed minimal drug release at pH 5 and pH 5.5 during the first hour, while no drug was released at physiological pH 7.4 after 4 hours, indicating that long-term exposure to ZIF-8 at alkaline pH can lead to gradual release of the loaded material [24, 72, 73]. It was concluded that ZIF-8 shows promise as a material for drug protection and delivery, and encapsulated ZIF-8 materials can be stored in normal or physiological media for a specified time.

4. Conclusion

The results obtained from this investigation provide evidence that Gla@ZIF-8 can be successfully synthesized using a one-pot method at ambient temperature while requiring minimal energy input. This signifies the practicality of incorporating hydrophobic, less stable, and pH/temperature-sensitive organic compounds within the ZIF-8 framework. These findings have significant implications for the development of advanced nanomedicine designs in the future. ZIF-8 exhibited a significant drug loading capacity of approximately 98.7% for glabridin, indicating its potential as a promising drug delivery system. The synthesis of Glab@ZIF-8 was confirmed through the utilization of various analytical techniques, including UV—Vis and FTIR spectroscopy, XRD, SEM, and TEM. Additionally, TGA analysis demonstrated that only 32.14% of the composite degraded before it reached a temperature of 644°C. Furthermore, a substantial drug release of 89.76% from Glab@ZIF-8 was observed within a 72-hour timeframe in an acidic medium, surpassing the release observed in physiological medium at a pH of 7.4. Therefore, because of its faster drug release at lower pH, the composite material can also be tested in in vitro clinical studies, as designed for low-pH diseased cells. With respect to antibacterial potential, 25 µg/50 µL Glab@ZIF-8 had greater antibacterial activity against gram-positive *S. aureus* bacteria than against *E. coli*, and the MIC values were 31.2 µg and 62.5 µg, respectively. Significantly, Glab@ZIF-8 exhibited notable antibacterial efficacy, suggesting its potential as a viable alternative to current antibiotics for mitigating drug resistance among bacterial species. This finding highlights the possibility

of considering similar materials in future research endeavors aimed at combating antibiotic resistance. Furthermore, these results indicated that the encapsulation of Glab in ZIF-8 (a MOF) was important and could be advantageous for the preparation of new drugs for biomedical applications, e.g., drug delivery systems.

Declarations

Acknowledgement: The authors acknowledge the School of International Education and College of Life Science and Technology, Beijing University of Chemical Technology, Beijing, China, for providing an admirable and motivational research environment.

Conflict of interest: The authors declare that they have no conflict of interest.

Ethical Approval: This declaration is “not applicable”.

Funding: Authors thankls the National Natural Science Foundation of China (22078014) for financial support.

Availability of data and materials: The data generated or analyzed during the present study are not publicly available but are available from the corresponding author at a reasonable request.

Author Contribution

Conceptualization: Safdar Ali Amur, Najaf Ali Soomro and Liang Hao; Methodology: Safdar Ali Amur, Mingxia Wang and Muhammad Tariq; Formal analysis and investigation: Quratulain Khuhro, Naveed Karim and Junaid Munawar; Writing - original draft preparation: Safdar Ali Amur and Quratulain Khuhro; Writing - review and editing: Najaf Ali Soomro, Liang Hao and Muhammad Tariq; Funding acquisition: Liang Hao; Resources: Liang Hao; Supervision: Liang Hao.

References

1. M. Abers, S. Schroeder, L. Goelz, A. Sulser, T. St. Rose, K. Puchalski, J. Langland, BMC Complement Med Ther 21 (2021). https://doi.org/10.1186/s12906-021-03285-3
2. WHO, World Health Organization 61 (2014). https://doi.org/10.1007/s13312-014-0374-3
3. C.V. Guillamet, Intensive Care Med 43 (2017). https://doi.org/10.1007/s00134-015-4126-1
4. T. Cardoso, O. Ribeiro, I.C. Aragão, A. Costa-Pereira, A.E. Sarmento, BMC Infect Dis 12 (2012). https://doi.org/10.1186/1471-2334-12-375
5. E. Cerceo, S.B. Deitelzweig, B.M. Sherman, A.N. Amin, Microbial Drug Resistance 22 (2016). https://doi.org/10.1089/mdr.2015.0220
6. J.H. Rex, G.H. Talbot, M.J. Goldberger, B.I. Eisenstein, R.M. Echols, J.F. Tomayko, M.N. Dudley, A. Dane, Clinical Infectious Diseases 65 (2017). https://doi.org/10.1093/cid/cix246

7. X. Li, R. Guo, X. Zhang, X. Li, Sep Purif Technol 88 (2012). https://doi.org/10.1016/j.seppur.2011.12.018
8. J. Phie, S.M. Krishna, J. V. Moxon, S.M. Omer, R. Kinobe, J. Golledge, PLoS One 12 (2017). https://doi.org/10.1371/journal.pone.0181832
9. E. Mirtaheri, N. Namazi, M. Alizadeh, N. Sargheini, S. Karimi, Eur J Integr Med 7 (2015). https://doi.org/10.1016/j.eujim.2015.03.006
10. L. Roque, N. Duarte, M.R. Bronze, C. Garcia, J. Alopaeus, J. Molpeceres, E. Hagesaether, I. Tho, P. Rijo, C. Reis, Biofouling 34 (2018). https://doi.org/10.1080/08927014.2018.1514391
11. P. Sidhu, S. Shankargouda, A. Rath, P. Hesarghatta Ramamurthy, B. Fernandes, A. Kumar Singh, J Ayurveda Integr Med 11 (2020). https://doi.org/10.1016/j.jaim.2017.12.004
12. B. Goel, A. Sharma, N. Tripathi, N. Bhardwaj, B. Sahu, G. Kaur, B. Singh, S.K. Jain, Nat Prod Res 35 (2021). https://doi.org/10.1080/14786419.2020.1786830
13. A.S. Chakotiya, A. Tanwar, P. Srivastava, A. Narula, R.K. Sharma, Biomedicine and Pharmacotherapy 90 (2017). https://doi.org/10.1016/j.biopha.2017.03.055
14. H.S. Kim, K.S. Suh, D. Sul, B.J.O. Kim, S.K. Lee, W.W. Jung, Int J Mol Med 29 (2012). https://doi.org/10.3892/ijmm.2011.822
15. M. Ao, Y. Shi, Y. Cui, W. Guo, J. Wang, L. Yu, Nat Prod Commun 5 (2010). https://doi.org/10.1177/1934578x1000501214
16. J. Zhang, X. Wu, B. Zhong, Q. Liao, X. Wang, Y. Xie, X. He, Drug Des Devel Ther 17 (2023). https://doi.org/10.2147/DDDT.S385981
17. C.W. Hsieh, P.H. Li, I.C. Lu, T.H. Wang, J Oleo Sci 61 (2012). https://doi.org/10.5650/jos.61.483
18. N.A. Soomro, Q. Wu, S.A. Amur, H. Liang, A. Ur Rahman, Q. Yuan, Y. Wei, Colloids Surf B Biointerfaces 182 (2019). https://doi.org/10.1016/j.colsurfb.2019.110364
19. S.A. Amur, N.A. Soomro, Q. Khuhro, Y. Wei, H. Liang, Q. Yuan, J Drug Deliv Sci Technol 84 (2023). https://doi.org/10.1016/j.jddst.2023.104530
20. A. Tiwari, A. Singh, N. Garg, J.K. Randhawa, Sci Rep 7 (2017). https://doi.org/10.1038/s41598-017-12786-6
21. A.V.A. Mariadoss, K. Saravanakumar, A. Sathiyaseelan, K.V. Naveen, M.H. Wang, Microb Pathog 167 (2022). https://doi.org/10.1016/j.micpath.2022.105544
22. O.C. Farokhzad, R. Langer, ACS Nano 3 (2009). https://doi.org/10.1021/nn900002m
23. H.N. Abdelhamid, Curr Med Chem 28 (2021). https://doi.org/10.2174/0929867328666210608143703
24. R.S. Varma, A. Baul, R. Wadhwa, S. Gulati, Metal-Organic Frameworks (MOFs) as Catalysts, 2022. https://doi.org/10.1007/978-981-16-7959-9_1
25. S. Oh, S. Lee, G. Lee, M. Oh, Sci Rep 13 (2023). https://doi.org/10.1038/s41598-023-39507-6
26. R. Lehnert, F. Seel, ZAAC - Journal of Inorganic and General Chemistry 464 (1980). https://doi.org/10.1002/zaac.19804640117

27. B. Chen, Z. Yang, Y. Zhu, Y. Xia, J Mater Chem A Mater 2 (2014). https://doi.org/10.1039/c4ta02984d
28. A. Mittal, S. Gandhi, I. Roy, Sci Rep 12 (2022). https://doi.org/10.1038/s41598-022-14630-y
29. A. Phan, C.J. Doonan, F.J. Uribe-Romo, C.B. Knobler, M. Okeeffe, O.M. Yaghi, Acc Chem Res 43 (2010). https://doi.org/10.1021/ar900116g
30. S.R. Venna, J.B. Jasinski, M.A. Carreon, J Am Chem Soc 132 (2010). https://doi.org/10.1021/ja109268m
31. G. Lu, S. Li, Z. Guo, O.K. Farha, B.G. Hauser, X. Qi, Y. Wang, X. Wang, S. Han, X. Liu, J.S. Duchene, H. Zhang, Q. Zhang, X. Chen, J. Ma, S.C.J. Loo, W.D. Wei, Y. Yang, J.T. Hupp, F. Huo, Nat Chem 4 (2012). https://doi.org/10.1038/nchem.1272
32. C.Y. Sun, C. Qin, X.L. Wang, G.S. Yang, K.Z. Shao, Y.Q. Lan, Z.M. Su, P. Huang, C.G. Wang, E.B. Wang, Dalton Transactions 41 (2012). https://doi.org/10.1039/c2dt30357d
33. J. Jung, I.H. Lee, E. Lee, J. Park, S. Jon, Biomacromolecules 8 (2007). https://doi.org/10.1021/bm700517z
34. J. Zhuang, C.H. Kuo, L.Y. Chou, D.Y. Liu, E. Weerapana, C.K. Tsung, ACS Nano 8 (2014). https://doi.org/10.1021/nn406590q
35. T. Wang, S. Li, Z. Zou, L. Hai, X. Yang, X. Jia, A. Zhang, D. He, X. He, K. Wang, J Mater Chem B 6 (2018). https://doi.org/10.1039/c8tb00351c
36. K. Wang, M. Qian, H. Qi, Q. Gao, C. Zhang, Nanoscale 12 (2020). https://doi.org/10.1039/d0nr02149k
37. T.T. Chen, J.T. Yi, Y.Y. Zhao, X. Chu, J Am Chem Soc 140 (2018). https://doi.org/10.1021/jacs.8b04457
38. Y. Wei, J. Zhang, Y. Zhou, W. Bei, Y. Li, Q. Yuan, H. Liang, Carbohydr Polym 159 (2017). https://doi.org/10.1016/j.carbpol.2016.11.093
39. M. Taheri, D. Ashok, T. Sen, T.G. Enge, N.K. Verma, A. Tricoli, A. Lowe, D. R. Nisbet, T. Tsuzuki, Stability of ZIF-8 nanopowders in bacterial culture media and its implication for antibacterial properties, Chemical Engineering Journal 413 (2021). https://doi.org/10.1016/j.cej.2020.127511
40. N.A. Soomro, S.A. Amur, Y. Wei, A.H. Shah, M. Jiao, H. Liang, Q. Yuan, J Clust Sci 32 (2021) 1519–1529. https://doi.org/10.1007/s10876-020-01908-2
41. M. Liu, Z. Xing, Z. Li, W. Zhou, Coord Chem Rev 446 (2021). https://doi.org/10.1016/j.ccr.2021.214123
42. N. Liédana, A. Galve, C. Rubio, C. Téllez, J. Coronas, ACS Appl Mater Interfaces 4 (2012). https://doi.org/10.1021/am301365h
43. K. Shanker, A. Fatima, A.S. Negi, V.K. Gupta, M.P. Darokar, M.M. Gupta, S.P.S. Khanuja, Chromatographia 65 (2007). https://doi.org/10.1365/s10337-007-0230-x
44. X. Xia, X. Song, Y. Li, W. Hou, H. Lv, F. Li, Y. Li, J. Liu, X. Li, Front Bioeng Biotechnol 10 (2022). https://doi.org/10.3389/fbioe.2022.1026743
45. H. Kaur, G.C. Mohanta, V. Gupta, D. Kukkar, S. Tyagi, J Drug Deliv Sci Technol 41 (2017). https://doi.org/10.1016/j.jddst.2017.07.004

46. H. Zheng, Y. Zhang, L. Liu, W. Wan, P. Guo, A.M. Nyström, X. Zou, J Am Chem Soc 138 (2016). https://doi.org/10.1021/jacs.5b11720
47. O. Abuzalat, H. Tantawy, M. Basuni, M.H. Alkordi, A. Baraka, RSC Adv 12 (2022). https://doi.org/10.1039/d2ra00218c
48. M. Sandomierski, M. Jakubowski, M. Ratajczak, A. Voelkel, Sci Rep 12 (2022). https://doi.org/10.1038/s41598-022-13187-0
49. R.N. Moussawi, D. Patra, RSC Adv 6 (2016). https://doi.org/10.1039/c5ra20221c
50. M.J. Mitchell, M.M. Billingsley, R.M. Haley, M.E. Wechsler, N.A. Peppas, R. Langer, Nat Rev Drug Discov 20 (2021). https://doi.org/10.1038/s41573-020-0090-8
51. D.J. Pochapski, C. Carvalho Dos Santos, G.W. Leite, S.H. Pulcinelli, C.V. Santilli, Langmuir 37 (2021). https://doi.org/10.1021/acs.langmuir.1c02056
52. J. Ma, K. Li, S. Gu, RSC Adv 12 (2022). https://doi.org/10.1039/d1ra08996j
53. D.P. Linklater, V.A. Baulin, S. Juodkazis, R.J. Crawford, P. Stoodley, E.P. Ivanova, Nat Rev Microbiol 19 (2021). https://doi.org/10.1038/s41579-020-0414-z
54. Q. Zhang, H. Zhou, P. Jiang, X. Xiao, J Hazard Mater 455 (2023). https://doi.org/10.1016/j.jhazmat.2023.131658
55. L. Harini, S. Srivastava, G.P. Gnanakumar, B. Karthikeyan, C. Ross, V. Krishnakumar, V.R. Kannan, K. Sundar, T. Kathiresan, Oncotarget 10 (2019). https://doi.org/10.18632/oncotarget.26623
56. S. Sanaei-Rad, M.A. Ghasemzadeh, S.M.H. Razavian, Sci Rep 11 (2021). https://doi.org/10.1038/s41598-021-98133-2
57. P. Gao, Q. Tong, J. Lv, Y. Wang, Y. Ma, Comput Phys Commun 213 (2017). https://doi.org/10.1016/j.cpc.2016.11.007
58. H. Bux, A. Feldhoff, J. Cravillon, M. Wiebcke, Y.S. Li, J. Caro, Chemistry of Materials 23 (2011). https://doi.org/10.1021/cm200555s
59. P. Jiang, K. Yu, H. Yuan, R. He, M. Sun, F. Tao, L. Wang, W. Zhu, J Mater Chem A Mater 9 (2021). https://doi.org/10.1039/d1ta00386k
60. R. Sacourbaravi, Z. Ansari-Asl, M. Kooti, V. Nobakht, E. Darabpour, J Inorg Organomet Polym Mater 30 (2020). https://doi.org/10.1007/s10904-020-01601-x
61. J. Yao, M. He, K. Wang, R. Chen, Z. Zhong, H. Wang, CrystEngComm 15 (2013). https://doi.org/10.1039/c3ce27093a
62. H.A. Khan, A. Ahmad, R. Mehboob, Asian Pac J Trop Biomed 5 (2015). https://doi.org/10.1016/j.apjtb.2015.05.001
63. G. Martelli, D. Giacomini, Eur J Med Chem 158 (2018). https://doi.org/10.1016/j.ejmech.2018.09.009
64. V.K. Gupta, A. Fatima, U. Faridi, A.S. Negi, K. Shanker, J.K. Kumar, N. Rahuja, S. Luqman, B.S. Sisodia, D. Saikia, M.P. Darokar, S.P.S. Khanuja, J Ethnopharmacol 116 (2008). https://doi.org/10.1016/j.jep.2007.11.037

65. D.B. Adimpong, K.I. Sørensen, L. Thorsen, B. Stuer-Lauridsen, W.S. Abdelgadir, D.S. Nielsen, P.M.F. Derkx, L. Jespersen, Appl Environ Microbiol 78 (2012). https://doi.org/10.1128/AEM.00730-12
66. A.P. Richter, J.S. Brown, B. Bharti, A. Wang, S. Gangwal, K. Houck, E.A. Cohen Hubal, V.N. Paunov, S.D. Stoyanov, O.D. Velev, Nat Nanotechnol 10 (2015). https://doi.org/10.1038/nnano.2015.141
67. G. Wyszogrodzka, B. Marszałek, B. Gil, P. Dorozyński, Drug Discov Today 21 (2016). https://doi.org/10.1016/j.drudis.2016.04.009
68. Z. Breijyeh, B. Jubeh, R. Karaman, Molecules 25 (2020). https://doi.org/10.3390/molecules25061340
69. M.P. Mingeot-Leclercq, J.L. Décout, Medchemcomm 7 (2016). https://doi.org/10.1039/c5md00503e
70. R.M. Epand, C. Walker, R.F. Epand, N.A. Magarvey, Biochim Biophys Acta Biomembr 1858 (2016). https://doi.org/10.1016/j.bbamem.2015.10.018
71. E. Sánchez-López, D. Gomes, G. Esteruelas, L. Bonilla, A.L. Lopez-Machado, R. Galindo, A. Cano, M. Espina, M. Ettcheto, A. Camins, A.M. Silva, A. Durazzo, A. Santini, M.L. Garcia, E.B. Souto, Nanomaterials 10 (2020). https://doi.org/10.3390/nano10020292.
72. O.M. Yaghi, M.J. Kalmutzki, C.S. Diercks, Introduction to Reticular Chemistry, (Wiley-VCH Verlag GmbH & Co. KGaA, 2019), pp. 1-27. https://doi.org/10.1002/9783527821099
73. H.D. Lawson, S.P. Walton, C. Chan, ACS Appl Mater Interfaces 13 (2021). https://doi.org/10.1021/acsami.1c01089

Figures

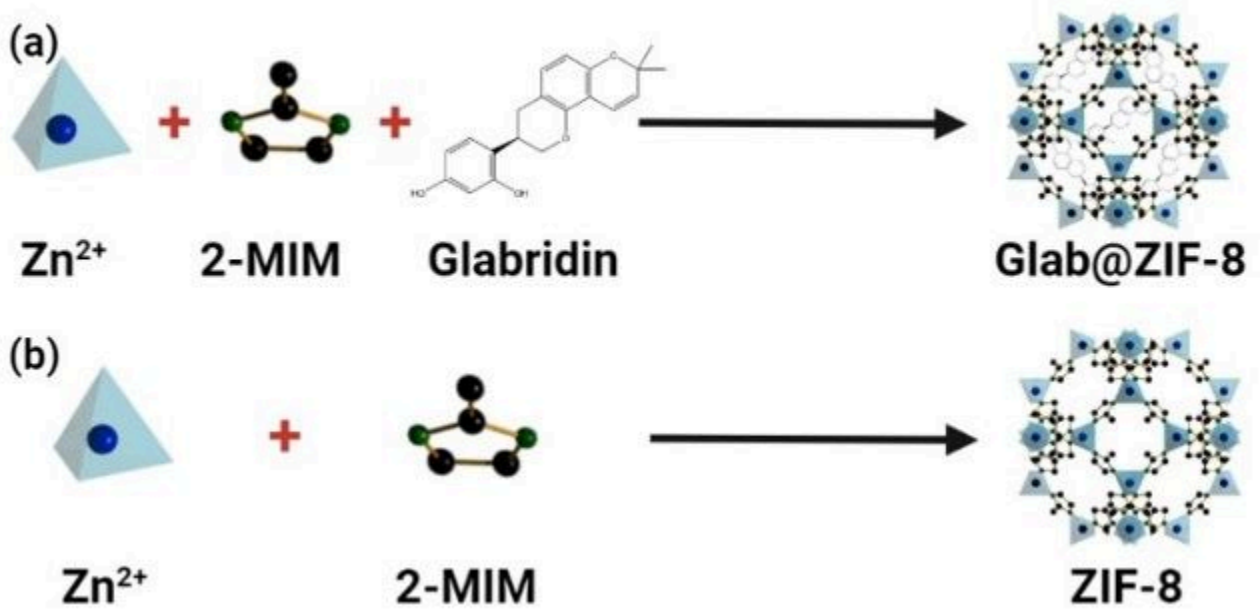

Figure 1

Schematic representation of synthesis of (a) Glab@ZIF-8 and (b) ZIF-8 nanoparticles

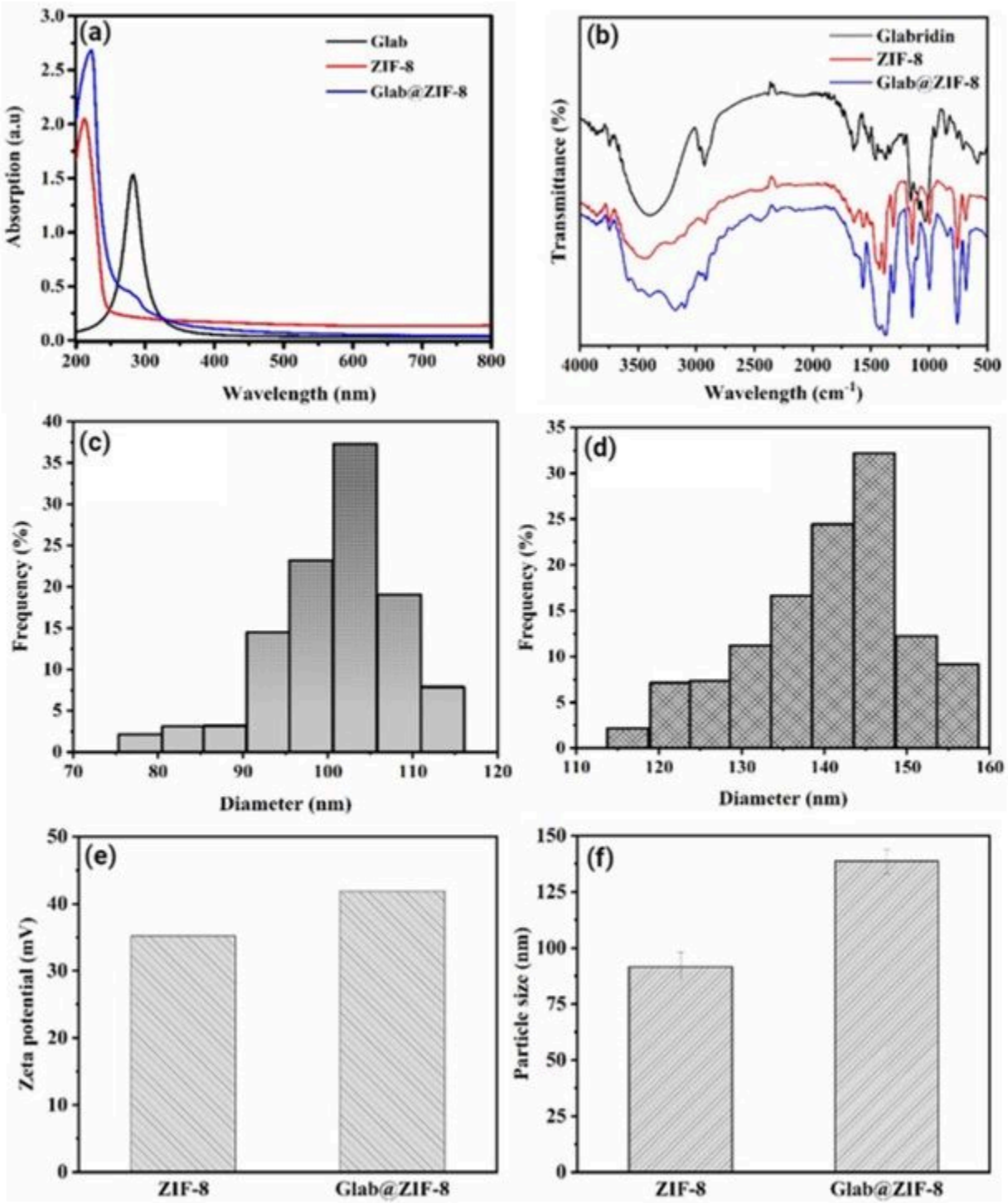

Figure 2

Shows the; (a) UV—vis analysis, (b) FTIR analysis; Hydrodynamic diameter size distributions of particles (c) ZIF-8, (d) Glab@ZIF-8; (e) Zeta potential (mV) and (f) Particle size (nm)

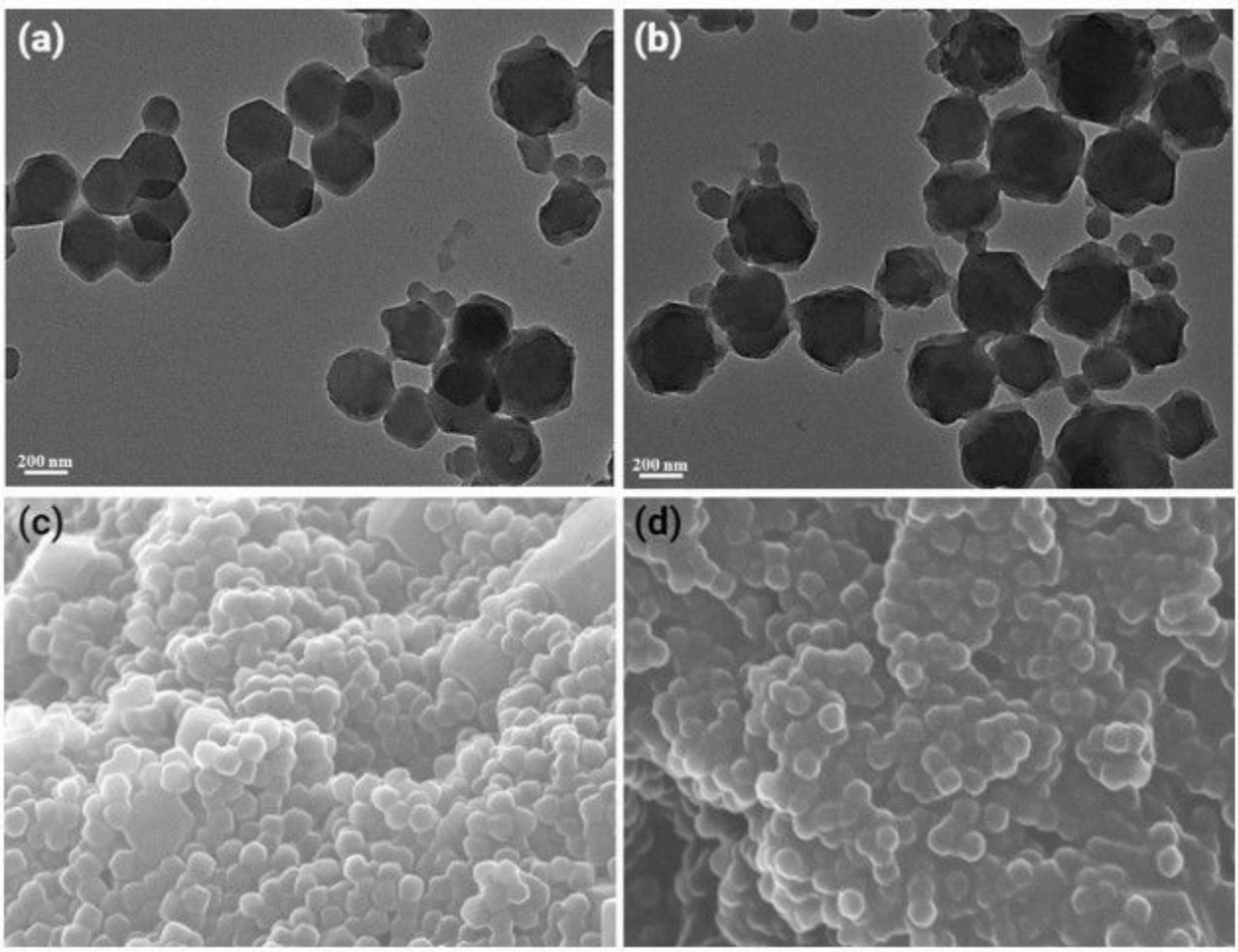

Figure 3

TEM and SEM images of the (a, c) ZIF-8 and (b, d) Glab@ZIF-8 nanoparticles

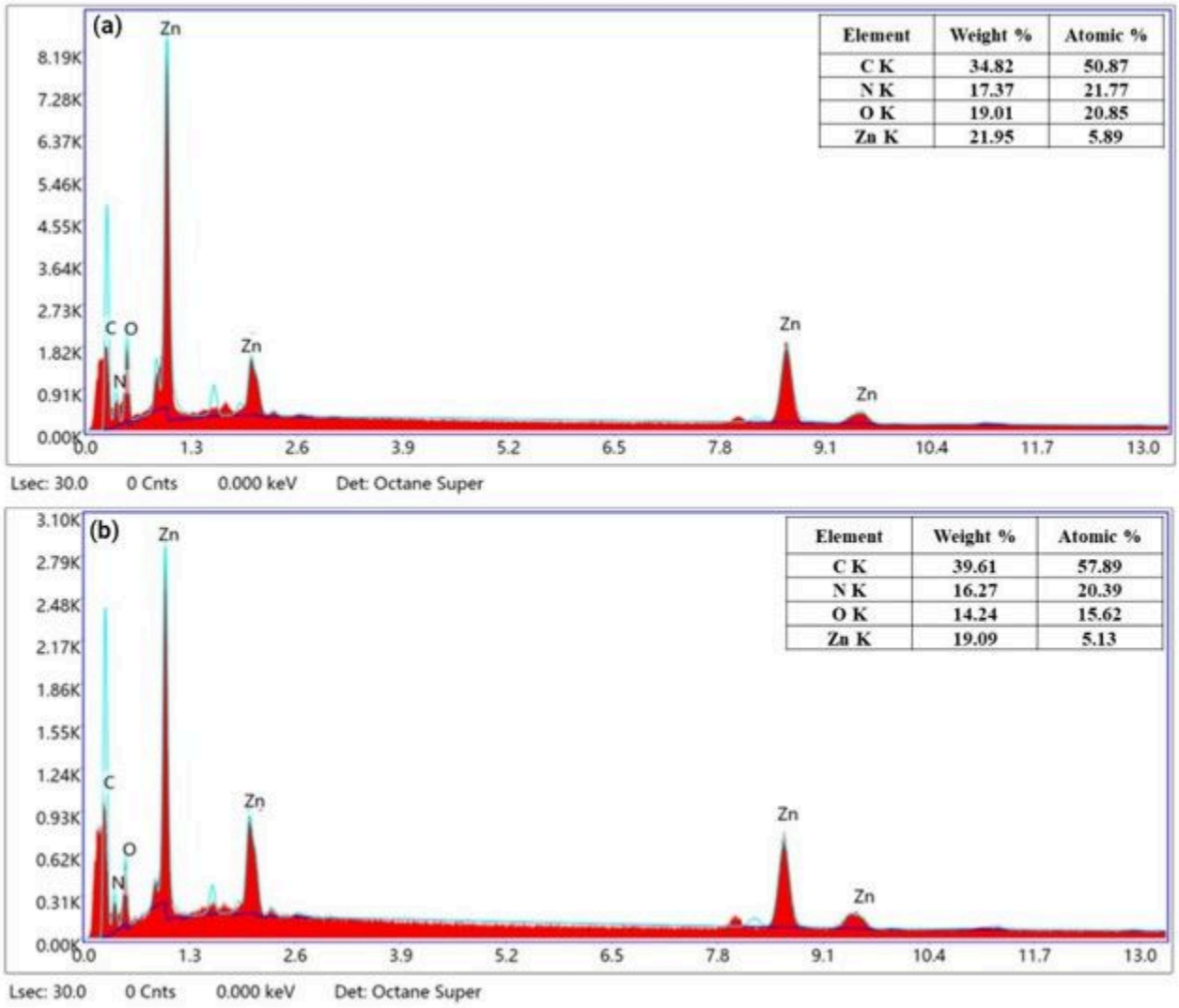

Element	Weight %	Atomic %
C K	34.82	50.87
N K	17.37	21.77
O K	19.01	20.85
Zn K	21.95	5.89

Element	Weight %	Atomic %
C K	39.61	57.89
N K	16.27	20.39
O K	14.24	15.62
Zn K	19.09	5.13

Figure 4

EDX elemental mapping of (a) ZIF-8 and (b) Glab@ZIF-8 nanoparticles

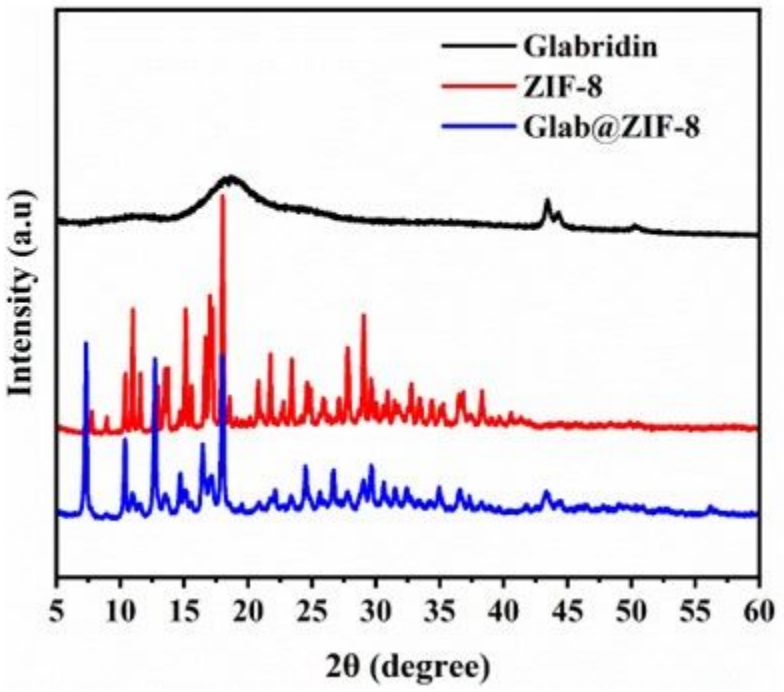

Figure 5

X-ray diffraction analysis of glabridin, ZIF-8 and Glab@ZIF-8 materials

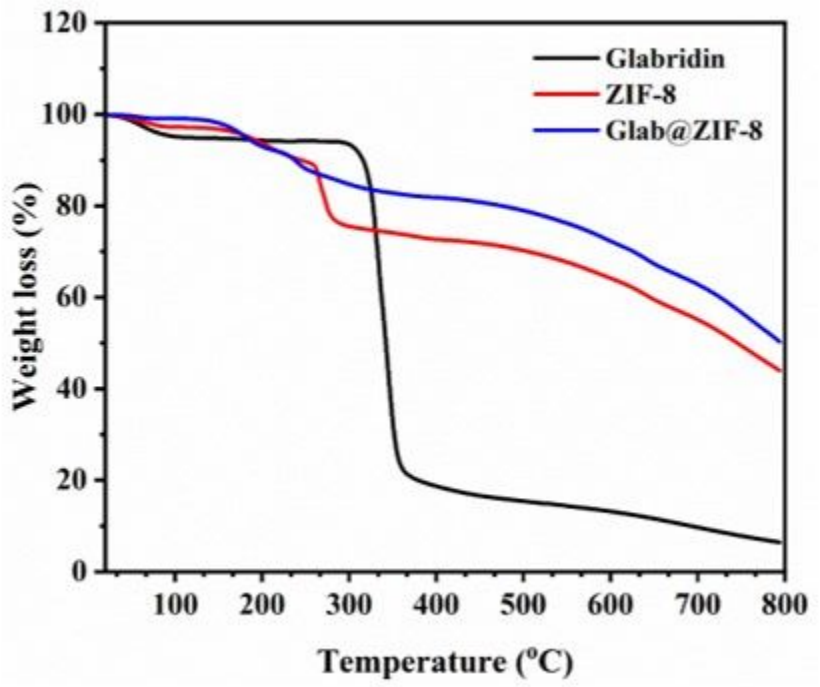

Figure 6

Thermogravimetric analysis of glabridin, ZIF-8 and Glab@ZIF-8 materials

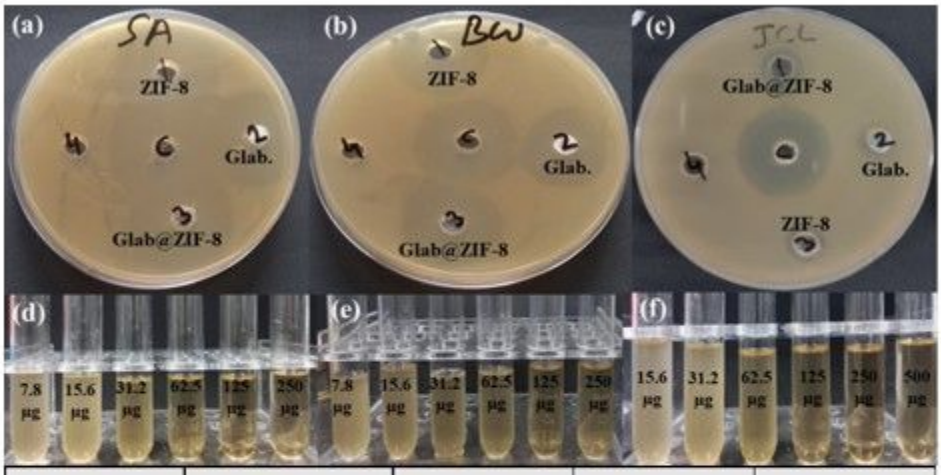

Bacteria Strains	Glab@ZIF-8 25 µg/50 µL	ZIF-8 50 µg/100 µL	Glab 50 µg/100 µL	Ampicillin 25 µg/50 µL
	Inhibition Zones (mm)			
S. aureus	26±0.01	17±0.01	15±0.03	27±0.03
E. coli (BW25113/F)	23±0.02	13±0.03	12±0.01	23±0.03
Bacillus subtilis (JCL16)	11±0.01	7.9±0.01	7±0.01	20±0.01

Figure 7

Antibacterial activity of the glabridin, ZIF-8 and Glab@ZIF-8 materials

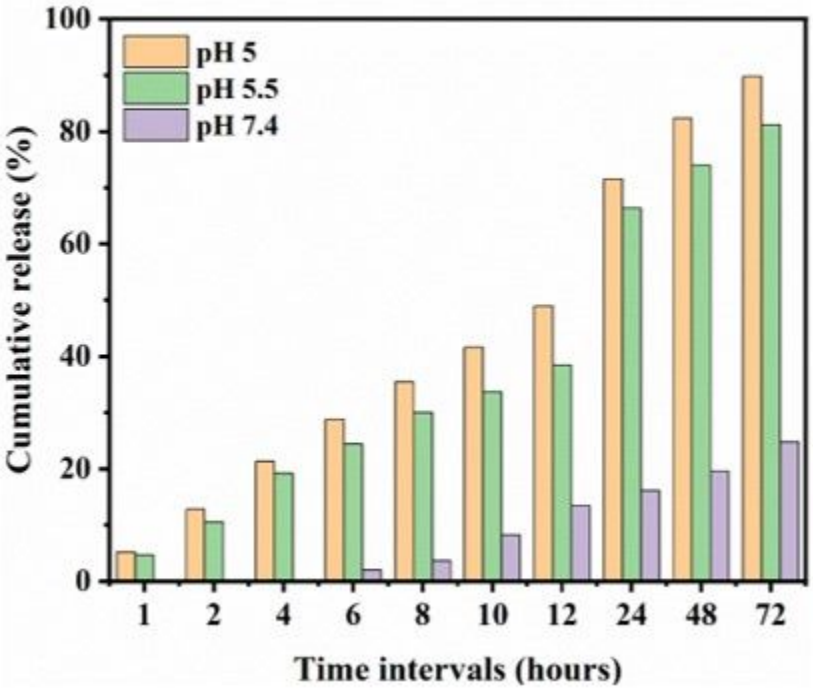

Figure 8

Drug (Glab) release profile from the Glab@ZIF-8 nanoparticles

Supplementary Files

This is a list of supplementary files associated with this preprint. Click to download.

- SupplementaryData.docx